Supporting Information

Liquid Sulfur Impregnation of Microporous Carbon Accelerated by Nanoscale Interfacial Effects

Tod A Pascal*, Irune Villaluenga, Kevin H. Wujcik, Didier Devaux, Xi Jiang, Dunyang (Rita) Wang, Nitash Balsara and David Prendergast*

[a]Molecular Foundry, Lawrence Berkeley National Lab, Berkeley, CA 94720

[b]Department of Chemical and Biomolecular Engineering, University of California, Berkeley, California 94720, USA

[c]Materials Sciences Division, Lawrence Berkeley National Laboratory, Berkeley, California 94720, USA

[d]Department of Materials Science and Engineering, University of California, Berkeley, California 94720, USA

[e]Energy Technologies Area, Lawrence Berkeley National Laboratory, Berkeley, California 94720, USA

*Corresponding authors: tapascal@lbl.gov (T.A.P) or dgprendergast@lbl.gob (D.P)

METHODS

Theoretical

Density Functional Theory Potential Energy Calculations

The binding energy of an isolated sulfur molecule on a graphene sheet (5x4 unit cell, 21.4x19.7 Å^2) was calculated from density functional theory calculations using the Vienna Ab Initio Simulation Package (VASP)[1, 2]. Two sets structure were considered: 1) the z projection of the S_8 center of mass, displaced from the graphene sheet 3.0 – 12.0Å in 0.1 Å increments and 2) the rotational barrier of an S_8 molecule on graphene at its equilibrium z displacement, from 0 – 180^o in 5^o increments. Single point energy calculations were performed with the exchange-correlation energy approximated by the following functionals employing the general gradient approximations: 1) PBE[3] 2) PBE with the DFT-D2 empirical corrections of Grimme et al.[4] 3) the self-consistent van der Waals vd-DF2[5] 3) the self-consistent van der Waals optB88-vdW[6].

Forcefield Fitting

We developed a force field for describing the carbon/sulfur interactions (termed the Molecular Foundry Force Field Carbon – Sulfur – MF[3]:C-S) by fitting to the vdW-DF2 binding energy curves. We chose a Buckingham analytic potential $E = Ae^{-r/\rho} - \frac{C}{r^6}$, which we think has the appropriate physics, i.e. an exponentially decaying Pauli-repulsion and a 1/r^6 London dispersion terms. We employed least squares fitting in a Newton-Raphson minimization scheme. Here, we let $\{\zeta\} = \{R, E\}$ be the set of observables we require the forcefield to reproduce, i.e.

(1)

is a function of the plane-plane distance (R) and the binding energy from DFT (E).

We then minimize the residual function:

$$R(\{\zeta\}) = \sum_{i=1}^{n} w_i \left[R_i^{calc}(\{\zeta\}) - R_i^{obs}(\{\zeta\})\right]^2$$

(2)

where N is the number of confirmations used in the fit and w_i is the weighting factor. Typical values for weighting factor are 10 for the distances and 100 for the energies. The resulting forcefield parameters are given in table S1.

Classical Molecular Dynamics (CMD) Simulations

CMD simulations were performed using the LAMMPS MD engine[7, 8]. Five types of systems were considered: 1) bulk sulfur comprising 696 molecules initiated from a 4x4x2 supercell of α-sulfur crystal unit cell 2) a 2D periodic slab of 696 sulfur molecule with 10nm vacuum 3) a 3D periodic slab on top of 2 graphene sheets. We attached a harmonic spring to the center of mass of each graphene sheet with force constant k = 500 kJ/mol/Å^2 and equilibrium distance r = 2nm to ensure no interactions between the sulfur surfaces in the z – direction. 4) a 3D periodic cylindrical nanopore, comprising carbon nanotubes of various radii (see figure S1b) capped by two parallel graphene sheets (10nm separation – figure S1a). The center of mass of the nanopore was constrained during the MD simulation. 5) sulfur molecules inside infinite 10nm carbon nanotubes, where we determined the optimal density by equilibrating the internal pressure to 1 bar by extracting/inserting molecules at each temperature.

We described the sulfur – sulfur interactions using the forcefield of Ballone and Jones[9], the graphene – graphene interactions using the QMFF-Cx forcefield[10] and the graphene – sulfur interactions using the MF^3:C-S forcefield field developed in this work. We ensured that the van der Waals energies and forces correctly converged to zero at the 1.2nm cutoff by employing a cubic spline from 1.1nm, preventing any energy drift that may occur due to inconsistent forces.

The systems were equilibrated according to our previous studies[11-13]: briefly, after initial conjugant gradient minimization at a force tolerance of 10^{-4} kcal/mol/A^2, the system was slowly heated from 0K to 298K with a Langevin thermostat in the constant temperature, constant volume micro-canonical (NVT) ensemble. The temperature coupling constant was 0.1 ps and the simulation timestep was 1.0fs.

For all systems other than the 2D periodic sulfur/vacuum calculation, this equilibration was followed by 10ns of constant-pressure (iso-baric), constant-temperature (NPT) dynamics at the required temperature and 1 atm. The temperature coupling constant was 0.1ps while the pressure piston constant was 2.0 ps. The equations of motion used are those of Shinoda et al.[14], which combine the hydrostatic equations of Martyna et al.[15] with the strain energy proposed by Parrinello and Rahman[16]. The time integration schemes closely follow the time-reversible measure-preserving Verlet integrators derived by Tuckerman et al.[17].
Production dynamics were then evolved for a further 25ns in the NVT ensemble. Snapshots of the system (atomic positions and velocities) were save every 10ps.

Free Energy and Surface Energy Calculations

Uncorrelated snapshots of the production MD simulation, 1ns apart (a total of 25 separate calculations), were subjected to a further 40ps of NVT MD simulations, saving the atomic coordinates and positions every 2fs. For each 40ps trajectory, the entropy of the sulfur molecules as well as the zero-point energy and heat capacity corrections to the enthalpy was calculated using an external code employing the Two-Phase Thermodynamics methods of Goddard and coworkers[18-20], employing the recent memory functions corrections[21]. In the case of the nanopore,

we separately considered the thermodynamics of the internal and external sulfur molecules, with the internal molecules defined as those that stayed within the 5Å of the pore entrance during the entire 40ps of dynamics. Molecules that entered and exited the pore entrance were ignored in this analysis.

First Principles Molecular Dynamics (FPMD) Simulations

A unit cell comprising a graphene sheet (3x4 unit cell) with 32 sulfur molecules (initial cell dimensions: 12.8x9.9x64 $Å^3$) was constructed and used as input a FPMD simulation, performed using a modified version of the mixed Gaussian and plane wave code CP2K/Quickstep.[22, 23] We employed a triple-ζ basis set with two additional sets of polarization functions (TZV2P)[24] and a 320 Ry plane-wave cutoff. The PBE functional was employed[3], and the Brillouin zone sampled at the Γ-point only, as is customary and reasonable for the wide-band gap, disordered, condensed phase system considered here. Interactions between the valence electrons and the ionic cores are described by norm-conserving pseudopotentials[25, 26]. Solutions to the Poisson equation are provided by an efficient Wavelet-based solver[27]. We overcome the poor description of the long-range dispersive forces within the PBE-GGA exchange-correlation functional by employing the D3 empirical corrections of Grimme and coworkers[4] We first equilibrated the system over 10ps of constant pressure (1bar), constant temperature (500K) dynamics using a Nose-Hoover thermostat (time relaxation constant of 0.1 ps) and an Anderson barostat (pressure relaxation constant of 1ps). The final cell parameters were 12.9x9.8x60.6 $Å^3$. This was followed by a 25 ps constant volume constant temperature (NVT) simulation, saving a snapshot of the system (atomic coordinates and velocities) at every step.

X-ray Absorption Spectroscopy Calculations

The final snapshot of our FPMD simulation was as input into an in-house code employing constrained-occupancy DFT calculations within the XCH approximation[28-30] to calculate the XAS spectra (256 individual calculations). Plane–wave pseudopotential calculations using ultrasoft pseudopotentials [31] were performed using the PWSCF code within the Quantum-ESPRESSO package[32]. We used a kinetic energy cut-off for electronic wave functions of 25 Ry and a density cut-off of 200 Ry The core-excited Kohn–Sham eigenspectrum was generated using the XCH approach[30]. Based on a numerically converged self-consistent charge density, we generated the unoccupied states for our XAS calculations non-self-consistently, sufficiently sampling the first Brillouin zone at the gamma point, employing an efficient implementation of the Shirley interpolation scheme[33] generalized to handle ultrasoft pseudopotentials[34]. Matrix elements were evaluated within the PAW frozen-core approximation[35]. Core-excited ultrasoft pseudopotentials and corresponding atomic orbitals were generated with the Vanderbilt code[31]. Each computed transition was convoluted with a 0.2 eV Gaussian function to produce continuous spectra.

Due to the use of pseudopotentials in our calculations (which means that we can only reliably compare the relative calculated excitation energies), we have developed an alignment scheme based on formation energy differences between the ground and core-excited states of the system and those of an isolated atom in the same simulation cell[29, 36]. Direct comparison to experiment is accomplished by first calibrating an unambiguous reference system. In the case of the sulfur compounds considered in this study, we rigidly shifted the first major peak in the sulfur K-edge XAS of an isolated S_2 molecule by +2467.5 eV to match the same in a gas phase experiment[37]. This empirical shift, is unique to the pseudopotentials employed in this study, and is applied to all subsequent calculated spectra. Previous experience has shown that this alignment scheme

predicts XAS peak positions to within ~0.1 eV[28, 29], which is typical of the experimental uncertainty in this energy range.

Experimental

Synthesis

Hollow carbon nanospheres were prepared by an ammonia aqueous solution (28 wt. %, 1.0 mL) that was added to a mixture of deionized water (3.3 mL) and ethanol (23.3 mL). After the mixture was stirred for 30 min at room temperature, tetraethyl orthosilicate (0.93 mL), resorcinol (0.13 g), and formalin (37 wt. %, 0.19 mL) were added to the solution at intervals of 10 min. The mixture was vigorously stirred for 24 h at room temperature and maintained at 100 ^{o}C for another 24 h in a Teflon autoclave. The product was then collected by centrifugation and dried. It was heated at 750 ^{o}C (5 ^{o}C/min) for 1 h under a flow of argon. The resulting black solid was dissolved an aqueous HF solution (15 wt.%) for 2 days to remove the silica core and get the porous hollow carbon nanospheres. The hollow carbon nanospheres were dissolved in HNO_3 at 80 ^{o}C for 2h to functionalize the surface of the carbon nanospheres with carboxylic groups (-COOH). This solution was centrifuged and washed with distilled water until pH was 7. The functionalized carbon nanospheres were dried under vacuum at 90 ^{o}C for 3 days. Finally, the composites of carbon nanospheres filled with sulfur were prepared by melt diffusion at 155 ^{o}C overnight to get 60 wt.% and 30 wt.% of sulfur.

Characterization

Thermogravimetric analysis (TGA) was carried out to determine the amount of sulfur in the carbon nanospheres. The samples were placed in an aluminum pan and heated up to 600 ^{o}C at 10 ^{o}C/min under a constant flow of argon gas. X-ray diffraction (XRD) of the sulfur, the hollow carbon nanospheres, and the composites carbon-sulfur nanospheres was performed using a Bruker AXS D8 X-ray diffractometer equipped with a GADDS area detector operating at Cu-Kα wavelength of λ= 1.54 Å. Samples were prepared on glass substrates. Pore volume and pore size of the carbon nanospheres was determined by nitrogen adsorption and desorption isotherms performed on a Tristar II adsorption instrument at 77 K. Both carbon nanospheres and carbon-sulfur nanospheres were dispersed in aqueous solution and applied to Lacey carbon film on gold grid for Energy-dispersive X-ray spectroscopy (EDS) characterizations. All micrographs for specimens were obtained by using TitanX scanning transmission electron microscopy (FEI, Netherlands) in high angle annular dark filed (HAADF) mode at 80 KeV, and elemental maps were collected simultaneously by using windowless EDS detector (Bruker, USA).

X-ray Absorption Spectroscopy

XAS measurements were performed at beamline 4-3 of the Stanford Synchrotron Radiation Lightsource. Preliminary XAS experiments were performed at beamline 9.3.1 of the Advanced Light Source (Lawrence Berkeley National Laboratory). Samples for XAS were prepared by pressing small amounts of the sulfur-impregnated carbon nanospheres to indium foil. Measurements were taken in electron yield mode by measuring the drain current produced by incident X-rays. The following step sizes were used to obtain each spectrum: 2440 eV to 2460 eV: 2.0 eV; 2460 eV to 2478 eV: 0.08 eV; 2478 eV to 2490 eV: 0.20 eV; 2490 eV to 2525 eV: 0.50 eV; and 2525 eV to 2575 eV: 5.0 eV. Each scan took roughly 8 minutes to collect and the spectra

shown in figure 4c are the average of three consecutive spectra obtained for each spectrum. The beam spot size was approximately 5mm x 2mm and was not moved between scans. The XAS measurement chamber was continuously flushed with helium. Calibration of the X-ray energy was performed using sodium thiosulfate (Sigma-Aldrich), setting the first peak maximum to 2472.02 eV. All measurements were taken at room temperature. Background subtraction and normalization of the spectra was performed using Athena.

TABLES

Table S1: Comparison of sulfur – Graphene binding between DFT and various analytic force field parameters

	DFT: vdW-DF2 functional	**MF[3] (this work)**	**[b,c]AMBER**	**[b,d]OPLS**	**[b,e]GAFF**	**[b,f]DREIDING**
S – C vdW parameters		[a]Buckingham: A = 1.5x10^5 kJ/mol ρ = 0.325/Å C = 4880 Å^6 kJ/mol	LJ 12-6: ε = 0.6135 σ = 3.48	LJ 12-6: ε = 0.66 σ = 3.575	LJ 12-6: ε = 0.614 σ = 3.48	LJ 12-6: ε = 0.757 σ = 3.53
COM distance (Å)	3.97	3.95	4.00	3.99	3.99	2.81
S_8 binding energy (kJ/mol)	-65.2 kJ/mol	-64.9	-62.5	-71.9	-63.4	-88.7

[a] Buckingham potential: $E = Ae^{-r/\rho} - \frac{C}{r^6}$

[b]Lennard Jones 12-6 potential $E = 4\varepsilon\left[\left(\frac{\sigma}{r}\right)^{12} - \left(\frac{\sigma}{r}\right)^{6}\right]$

[c] Using Lorentz–Berthelot combination rules: $\varepsilon_{S-C} = \sqrt{\varepsilon_{C-C} \times \varepsilon_{C-C}}, \sigma_{S-C} = \frac{1}{2}\left(\sigma_{C-C} + \sigma_{S-S}\right)$, Parameters from reference[38]

[d]reference[39]

[e]reference[40]

[f]Using geometric combination rules: $\varepsilon_{S-C} = \sqrt{\varepsilon_{C-C} \times \varepsilon_{C-C}}, \sigma_{S-C} = \sqrt{\sigma_{C-C} \times \sigma_{S-S}}$. Parameters from reference[41]

Table S2: Thermodynamics of sulfur molecules in the bulk, at the sulfur – air and sulfur –graphene interface and encapsulated in microporous carbon nanopores T = T_m = 390K

	Bulk		**0.71 nm CNT**		**1.25 nm CNT**		**2.1 nm CNT**		**Sulfur/Air**		**Sulfur/ Graphene**	
	avg	±	avg	±	avg	±	avg	±	avg	±	avg	±
G^0 (kJ/mol)	-130.28	0.25	-154.04	2.16	-152.23	0.77	-151.56	0.58	-120.55	0.31	-146.13	0.81
H^0 (kJ/mol)	2.28	0.05	-16.75	2.57	-23.45	1.41	-19.38	0.81	16.74	0.14	-16.64	0.86
S^0 (J/mol/K)	341.47	0.36	352.68	8.02	330.50	4.22	339.65	3.55	354.61	0.59	334.44	1.06
Cv (J/mol/K)	186.54	14.50	52.77	36.80	35.61	19.78	41.57	39.34	314.46	25.55	108.55	10.71
ρ (g/cm^3)	1.88	0.15	1.61	0.06	1.93	0.02	1.94	0.03			1.89	0.27

Dx10^5 (cm^2/s)	0.202	0.019	0.270	0.325	0.384	0.204	0.374	0.144	0.633	0.025	0.427	0.091

Table S3: Sulfur/graphene surface free energy $\gamma_{SL}(G)$ (mJ/m^2), surface enthalpy $\gamma_{SL}(H)$ and surface entropy $\gamma_{SL}(TS)$ and macroscopic contact angle theta Θ (degrees) for multi-layer graphene at T_m

#layers	**$\gamma_{SL}(G)$**	**±**	**$\gamma_{SL}(H)$**	**±**	**$\gamma_{SL}(TS)$**	**±**	**Θ**	**±**
1	-41.92	0.42	-46.88	0.46	-4.90	0.40	41.80	8.82
2	-41.00	0.99	-47.32	0.39	-6.28	1.12	43.18	8.92
3	-39.63	0.65	-48.00	0.45	-8.45	0.89	45.19	10.57
4	-38.57	0.81	-48.12	0.43	-9.42	1.15	46.69	18.06
6	-38.89	0.58	-48.09	0.39	-9.34	1.07	46.24	11.19

Table S4: Free energy per sulfur molecule (kJ/mol/molecule) as at various temperatures

T(K)	**Bulk**		**0.71 nm CNT**		**1.25 nm CNT**		**2.1 nm CNT**		**Sulfur/ Air**		**Sulfur/Graphene**	
	avg	±	avg	±	avg	±	avg	±	avg	±	avg	±
390	-130.28	0.25	-153.04	2.16	-151.23	0.77	-150.05	0.58	-120.55	0.31	-146.08	0.81
400	-133.59	0.34	-156.73	1.61	-156.22	1.17	-155.46	0.62	-125.00	0.35	-148.92	0.91
405	-135.51	0.36	-158.77	1.86	-157.50	0.99	-156.87	1.08	-126.32	0.26	-151.89	0.72
410	-137.29	0.24	-160.29	2.13	-159.87	1.30	-158.48	0.57	-128.16	0.30	-153.12	0.78
415	-139.07	0.27	-163.32	1.92	-161.10	0.99	-160.13	0.77	-129.81	0.25	-156.31	0.51
420	-140.83	0.26	-164.12	2.27	-162.71	1.28	-161.96	0.74	-132.50	0.29	-157.08	0.77
425	-142.76	0.23	-166.00	1.85	-164.28	0.98	-163.67	0.75	-133.26	0.26	-159.70	0.93
430	-144.54	0.25	-169.51	1.97	-167.49	1.37	-165.96	0.74	-136.06	0.31	-161.57	0.60

Table S5: Liquid sulfur/vacuum (γ_{lg}) and sulfur/graphene (γ_{sl}) surface free energies (mJ/m^2) and macroscopic contact angle Θ (degrees) at various temperatures

T(K)	**γ_{lg}**	**±**	**γ_{sl}**	**±**	**Θ**	**±**
390	56.23	1.42	-41.92	1.56	41.80	6.87
400	56.39	1.56	-40.68	1.61	43.83	7.35
405	58.05	1.15	-43.45	1.15	41.55	7.36
410	57.29	1.38	-42.01	1.18	42.84	6.94
415	57.13	1.14	-45.75	0.70	36.79	8.98
420	56.63	1.21	-43.13	0.98	40.40	9.08
425	56.37	1.04	-44.95	1.12	37.11	8.14
430	55.88	1.25	-45.18	0.66	36.04	9.45

FIGURES

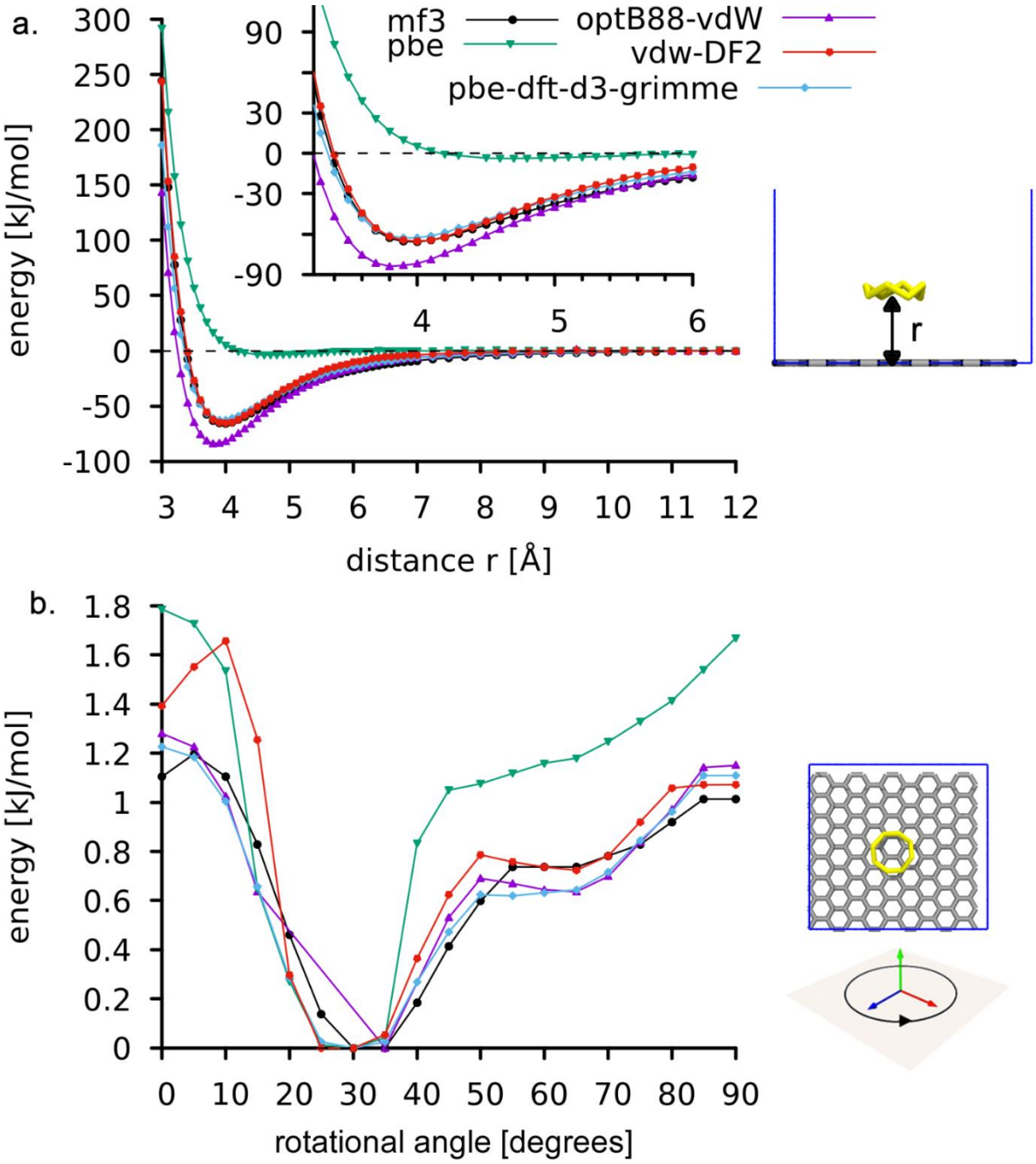

Figure S1: Sulfur – Carbon interactions. **a.** Binding energy of a single molecule of S_8 over graphene (schematically shown in right inset), obtained using various flavors of DFT GGA functionals (pbe: green, pbe-dft-d3-grimme: blue, vdw-DF2: red and the optB88-vdW: purple). The Molecular Foundry Forcefield (MF^3 - black) is fitted to reproduce the vdw-DF2 binding curve. **b.** Binding energy of a rotating S_8 molecule on graphene at the equilibrium distance.

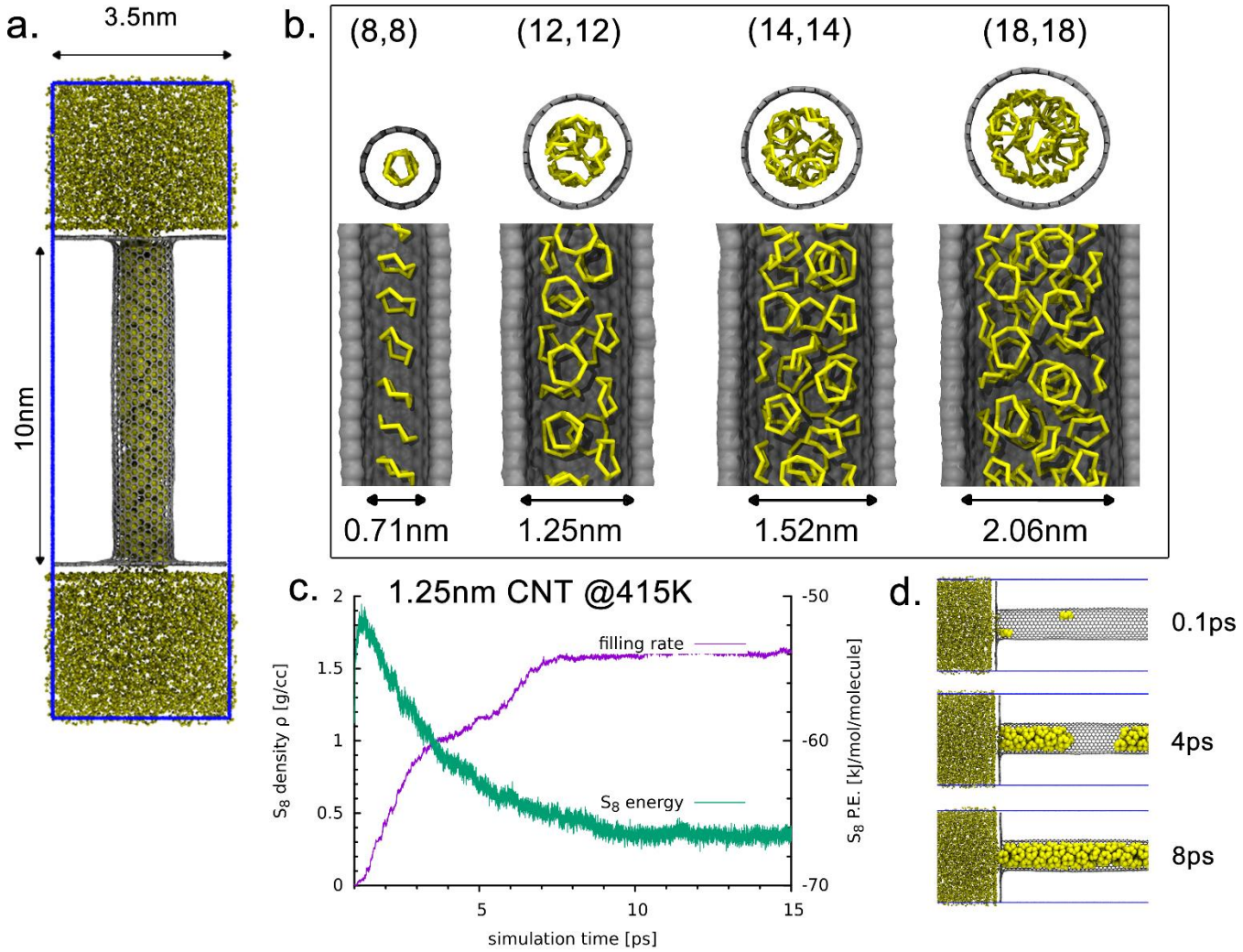

Figure S2: Structure and kinetics of sulfur intercalated in carbon nanotubes. **a.** Schematic of simulation cell. **b.** Equilibrium snapshots of various pores, showing the nanotube indices in brackets and the van der Waals radii. **c.** Density and potential energy per sulfur molecule during filling. **d.** Snapshots during filling.

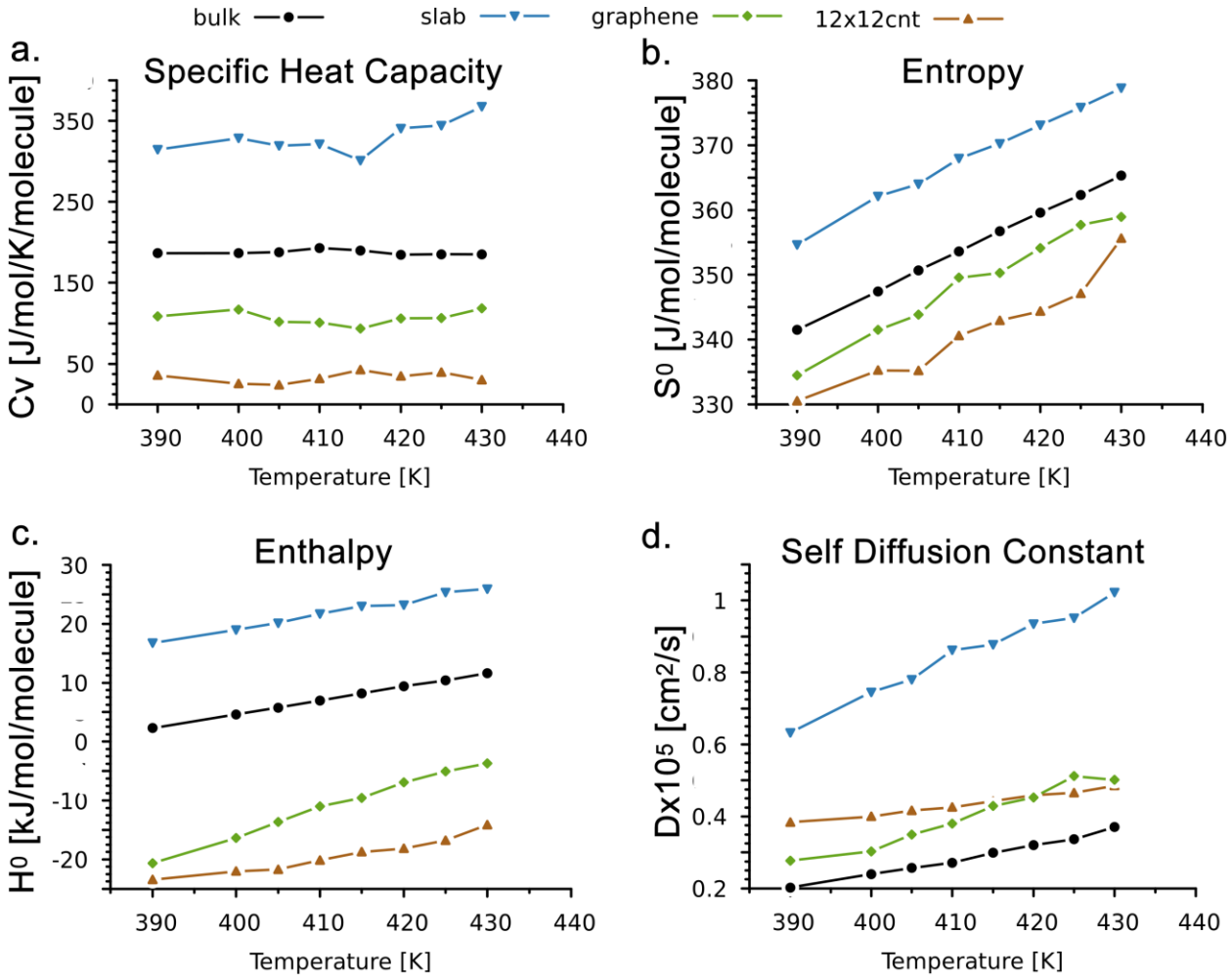

Figure S3: Temperature dependent sulfur equilibrium thermodynamics **a.** Per molecule constant volume specific heat capacity (C_v) of bulk liquid sulfur (black), interfacial sulfur at the vacuum interface (blue), interfacial sulfur on graphene (green) and encapsulated in a 1.6nm CNT (gold). **b.** Standard molar entropy S0 **c.** Molar enthalpy **d.** Self-diffusion constant

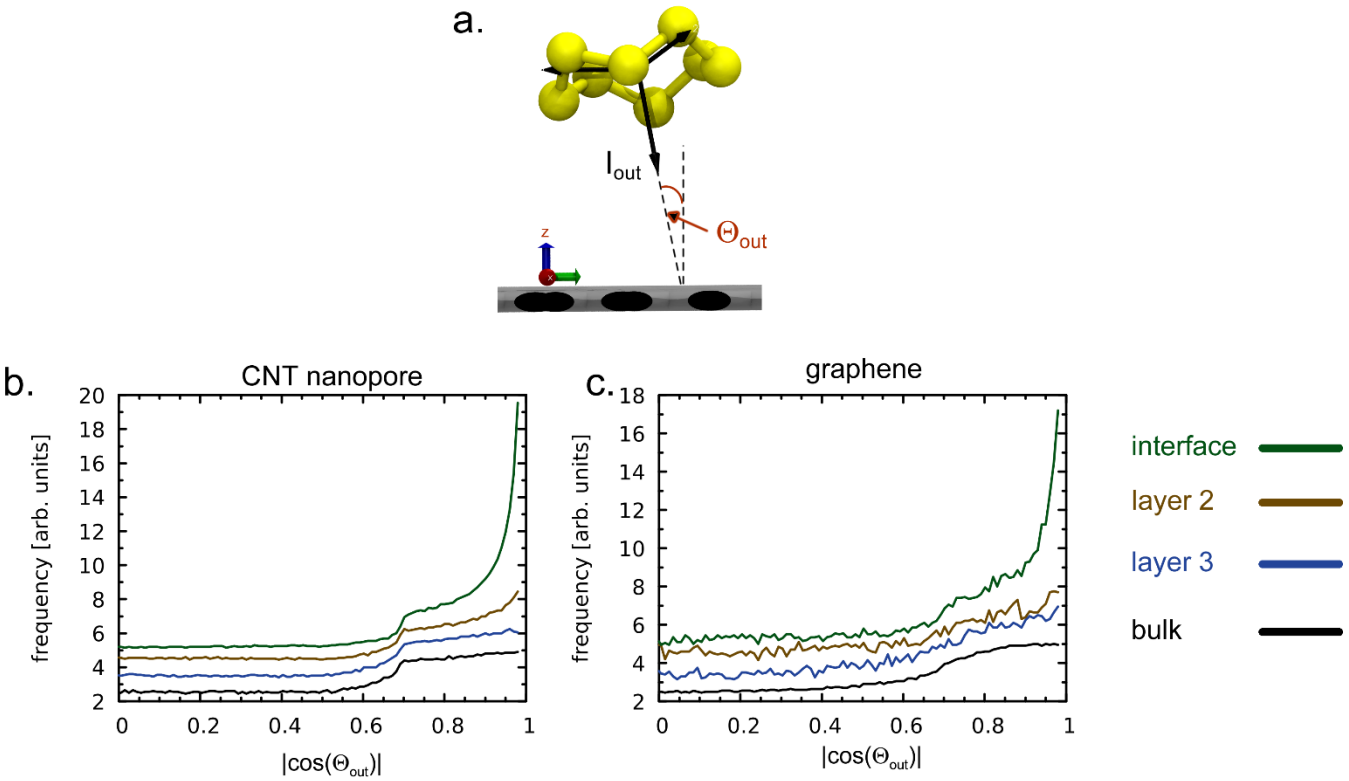

Figure S4 Sulfur orientation analysis on carbon. **a.** Schematic, illustrating the out-of-plane principle moments of inertia I_{out}. We record the absolute value of the angle with the Z-axis (Θ_{out}) each step during the production MD simulation. Note that a S_8 molecule lying flat on the interface is characterized by $|\cos(\Theta_{out})| = 1$. **b.** Θ_{out} distribution for S_8 molecules impregnated in a 5nm diameter carbon nanopore. The molecules are separated as a function of the radial distance of their center of mass from the CNT walls. The distribution for molecules in the 1st layer (labeled interface – green line), subsurface (layer 2 – brown line), sub-subsurface (layer 3 – blue line) and the bulk (layer 4 – black line) are offset by 2 for presentation purposes. **c.** Θ_{out} distribution for sulfur molecules at the planar graphene interface. Distributions for molecules in various vertical layers from the graphene surface are shown, using the same color scheme as previous.

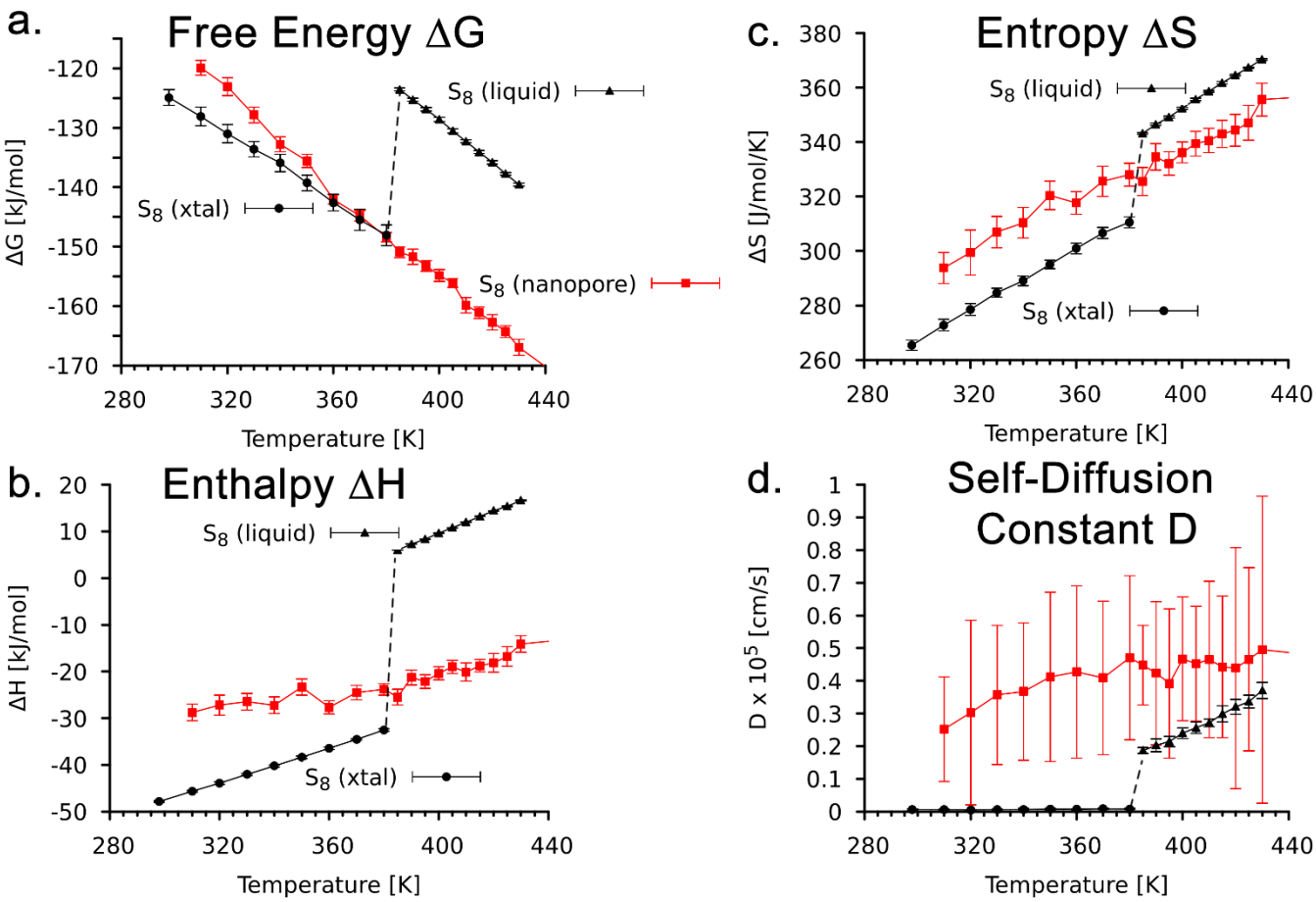

Figure S5: Comparison of the thermodynamics of sulfur encapsulated in a 1.25nm diameter nanoopore (red), the bulk crystal (black circles) and the bulk liquid (black triangles) **a.** Gibbs free energy ΔG [kJ/mol]. Our calculated data (points) is connected by straight lines for presentation purposes. The uncertainty in our calculated values (standard deviation 1σ) is indicated by vertical errorbars. The dashed vertical lines indicate the transition at the melting temperature T_m = 390K **b.** Enthalpy ΔH [kJ/mol] **c.** Entropy ΔS [J/mol/K] **d.** Self-diffusion constant Dx10^5 [cm/s]

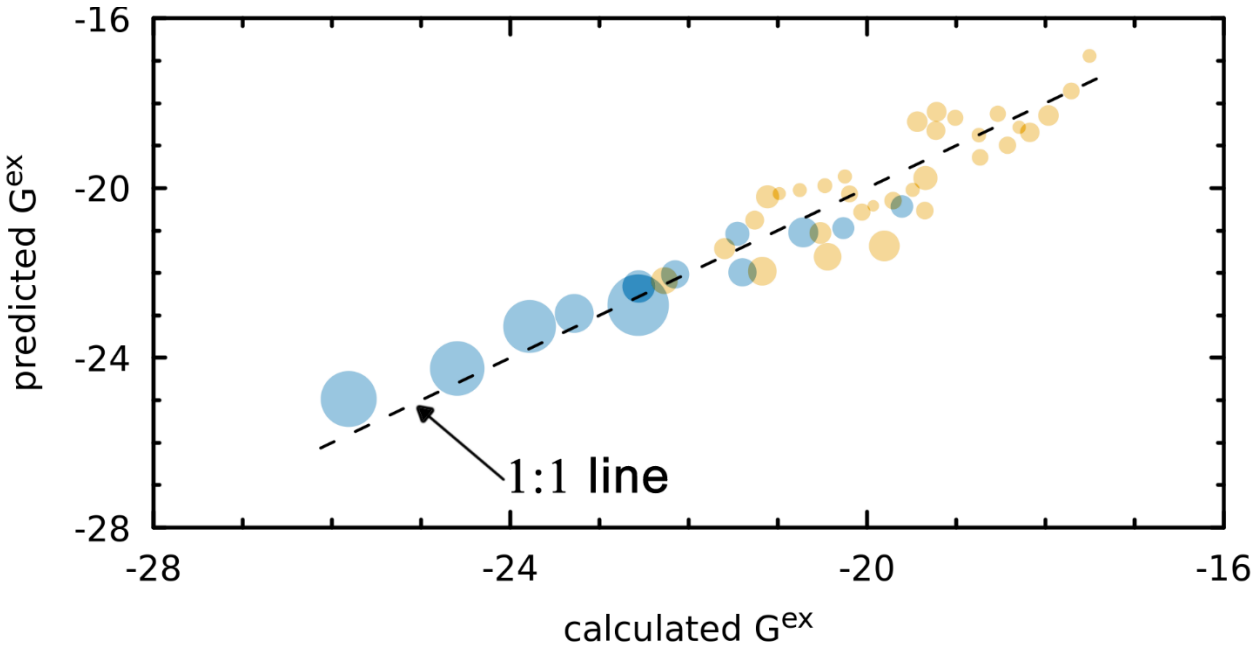

Figure S6: Excess free energy of sulfur encapsulated in carbon nanopores of radii r 0.7 – 3.0 nm compared to the predictions of our thermodynamic model from 390K – 430K. Microporous (r <2nm - blue) and mesoporous (r >2nm – yellow) nanopores are shown. The uncertainty in our calculations is indicated by the size of the filled circles. The dashed line represents 1:1 correlation. The correlation coefficient is 1.03.

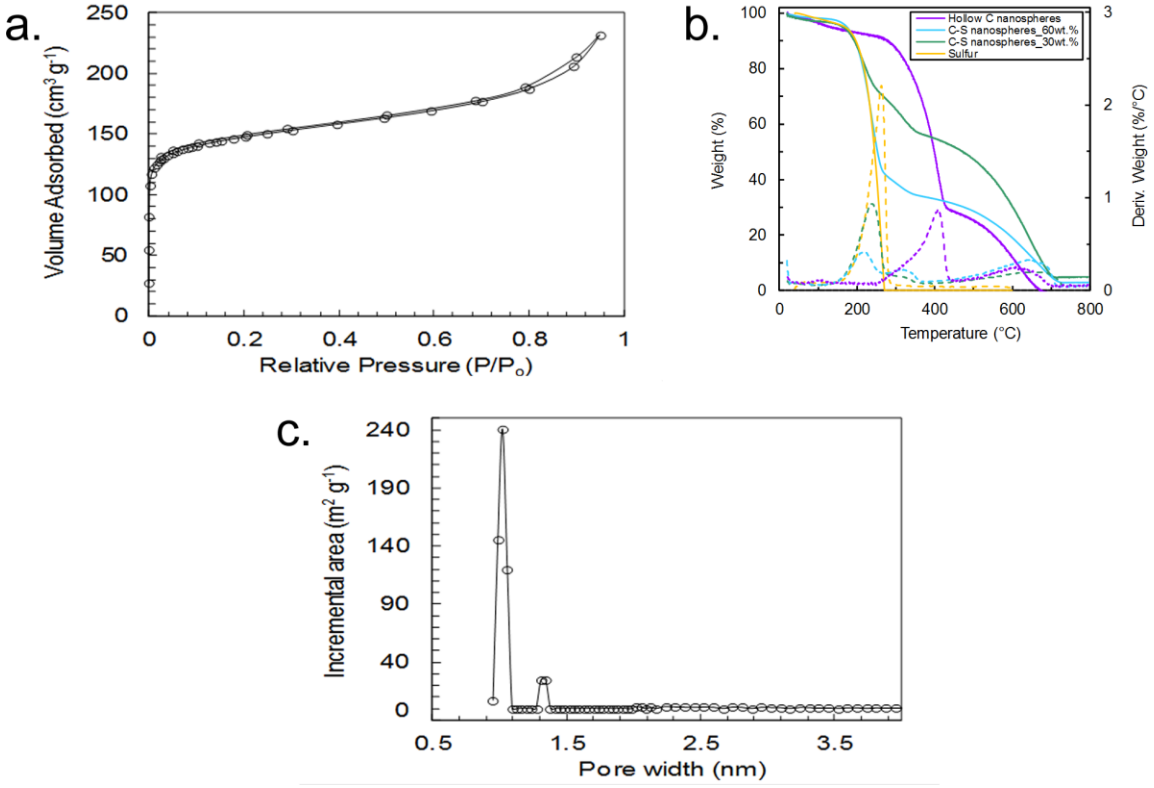

Figure S7: **a.** N_2 adsorption isotherm of the hollow carbon nanospheres. **b.** TGA thermograms of the sulfur, hollow carbon nanospheres, and carbon nanospheres with 60 wt.% and 30 wt.% of sulfur. **c.** Brunauer-Emmett-Teller (BET) pore size distribution analysis of the hollow carbon nanospheres, showing peaks between 1 – 1.3 nm.

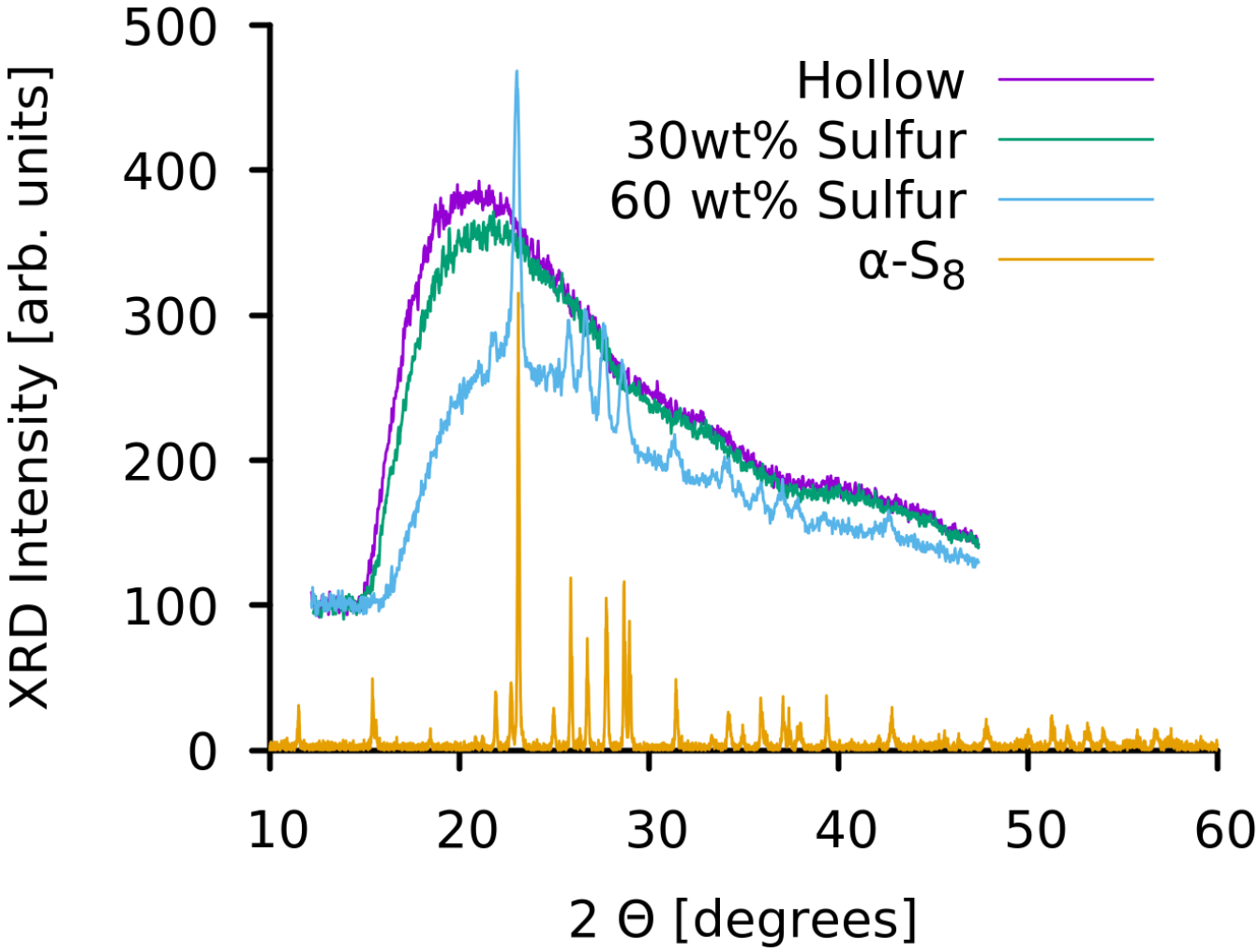

Figure S8: X-ray powder diffraction (XRD) analysis of the various nanospheres. The XRD of crystalline octasulfur (gold) is given as reference.

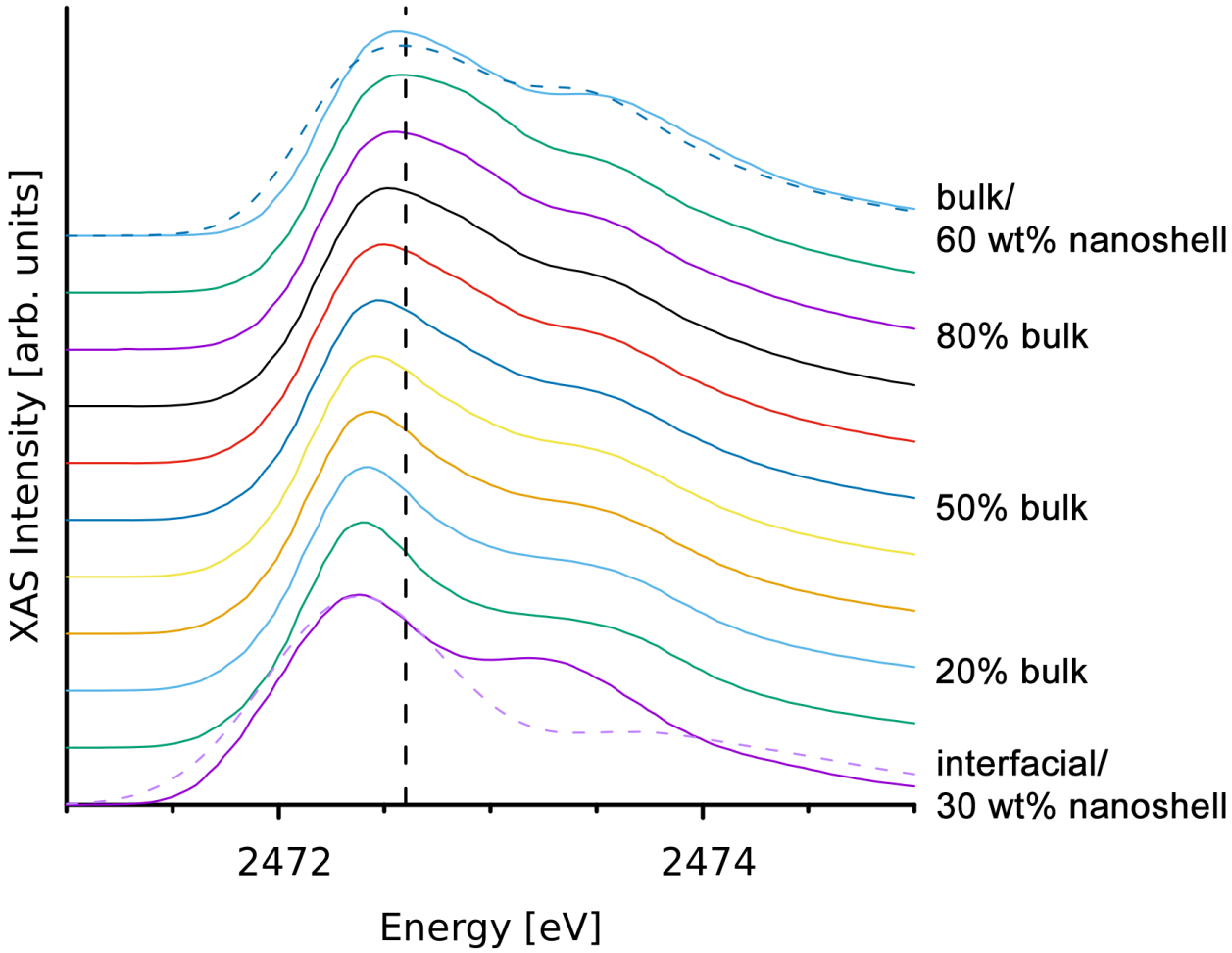

Figure S9: Simulated Sulfur K-edge XAS of systems with varying interfacial:bulk sulfur compositions. The XAS of the 30 wt% carbon nanoshell is well approximated by the interfacial sulfur spectrum, while 60 wt% sample corresponds to the bulk spectrum as indicated by the dashed lines.

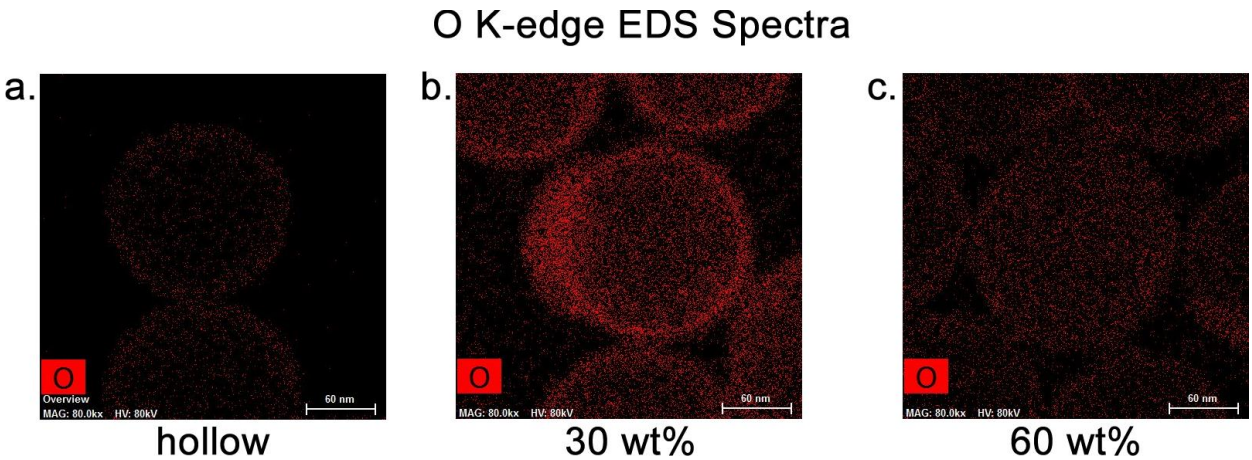

Figure S10: Oxygen K-edge energy dispersive X-ray spectroscopy (EDS) of carbon nanoshells loaded with sulfur to varying degrees: **a. 0 wt% (**hollow); **b.** 30 wt%; and **c.** 60 wt%.

REFERENCES

1. Kresse, G.; Furthmuller, J. *Comput. Mater. Sci.* **1996,** 6, 15-50.
2. Kresse, G.; Hafner, J. *Phys. Rev. B* **1993,** 47, 558-561.
3. Perdew, J. P.; Burke, K.; Ernzerhof, M. *Phys. Rev. Lett.* **1996,** 77, 3865-3868.
4. Grimme, S.; Antony, J.; Ehrlich, S.; Krieg, H. *J. Chem. Phys.* **2010,** 132, 154104-19.
5. Lee, K.; Murray, E. D.; Kong, L.; Lundqvist, B. I.; Langreth, D. C. *Phys. Rev. B* **2010,** 82, 081101.
6. Klimeš, J.; Bowler, D. R.; Michaelides, A. *J. Phys.: Condens. Matter* **2009,** 22, 022201.
7. Plimpton, S. J.; Pollock, R.; Stevens, M. In *Particle-Mesh Ewald and rRESPA for Parallel Molecular Dynamics Simulations*, Proc of the Eighth SIAM Conference on Parallel Processing for Scientific Computing, Minneapolis, MN 1997; Minneapolis, MN
8. Plimpton, S. *J. Comput. Phys.* **1995,** 117, 1-19.
9. Ballone, P.; Jones, R. O. *J. Chem. Phys.* **2003,** 119, 8704-8715.
10. Pascal, T. A.; Karasawa, N.; Goddard, W. A., 3rd. *J Chem Phys* **2010,** 133, 134114.
11. Maiti, P. K. P., Tod A.; Vaidehi, Nagarajan; Goddard, William A. *J. Nanosci. Nanotechnol.* **2007,** 7, 1712-1720.
12. Maiti, P. K.; Pascal, T. A.; Vaidehi, N.; Heo, J.; Goddard, W. A. *Biophys. J.* **2006,** 90, 1463-1479.
13. Maiti, P. K.; Pascal, T. A.; Vaidehi, N.; Goddard, W. A. *NUCLEIC ACIDS RES* **2004,** 32, 6047-6056.
14. Shinoda, W.; Shiga, M.; Mikami, M. *Physical Review B* **2004,** 69, -.
15. Martyna, G. J.; Tobias, D. J.; Klein, M. L. *J. Chem. Phys.* **1994,** 101, 4177-4189.
16. Parrinello, M.; Rahman, A. *Journal of Applied Physics* **1981,** 52, 7182-7190.
17. Tuckerman, M. E.; Alejandre, J.; Lopez-Rendon, R.; Jochim, A. L.; Martyna, G. J. *J Phys a-Math Gen* **2006,** 39, 5629-5651.
18. Pascal, T. A.; Lin, S. T.; Goddard, W. A., 3rd. *Physical chemistry chemical physics : PCCP* **2011,** 13, 169-81.
19. Lin, S.-T.; Maiti, P. K.; Goddard, W. A. *J. Phys. Chem. B* **2010,** 114, 8191-8198.
20. Lin, S. T.; Blanco, M.; Goddard, W. A. *J. Chem. Phys.* **2003,** 119, 11792-11805.
21. Desjarlais, M. P. *Phys. Rev. E* **2013,** 88, 062145.
22. Lippert, G.; Hutter, J.; Parrinello, M. *Mol Phys* **1997,** 92, 477-487.
23. VandeVondele, J.; Krack, M.; Mohamed, F.; Parrinello, M.; Chassaing, T.; Hutter, J. *Comput Phys Commun* **2005,** 167, 103-128.
24. VandeVondele, J.; Hutter, J. *J. Chem. Phys.* **2007,** 127, -.
25. Krack, M. *Theor Chem Acc* **2005,** 114, 145-152.
26. Goedecker, S.; Teter, M.; Hutter, J. *Phys. Rev. B* **1996,** 54, 1703-1710.
27. Genovese, L.; Deutsch, T.; Goedecker, S. *J. Chem. Phys.* **2007,** 127, -.
28. Pascal, T. A.; Boesenberg, U.; Kostecki, R.; Richardson, T. J.; Weng, T.-C.; Sokaras, D.; Nordlund, D.; McDermott, E.; Moewes, A.; Cabana, J.; Prendergast, D. *J. Chem. Phys.* **2014,** 140, 034107-034121.
29. England, A. H.; Duffin, A. M.; Schwartz, C. P.; Uejio, J. S.; Prendergast, D.; Saykally, R. J. *Chemical Physics Letters* **2011,** 514, 187-195.
30. Prendergast, D.; Galli, G. *Phys. Rev. Lett.* **2006,** 96, 215502.

31. Vanderbilt, D. *Phys. Rev. B* **1990,** 41, 7892-7895.
32. Giannozzi, P.; Baroni, S.; Bonini, N.; Calandra, M.; Car, R.; Cavazzoni, C.; Ceresoli, D.; Chiarotti, G. L.; Cococcioni, M.; Dabo, I. *J. Phys.: Condens. Matter* **2009,** 21, 395502.
33. Shirley, E. L. *Phys. Rev. B* **1996,** 54, 16464.
34. Prendergast, D.; Louie, S. G. *Physical Review B* **2009,** 80.
35. Taillefumier, M.; Cabaret, D.; Flank, A.-M.; Mauri, F. *Phys. Rev. B* **2002,** 66, 195107.
36. Jiang, P.; Prendergast, D.; Borondics, F.; Porsgaard, S.; Giovanetti, L.; Pach, E.; Newberg, J.; Bluhm, H.; Besenbacher, F.; Salmeron, M. *J. Chem. Phys.* **2013,** 138, 024704-6.
37. Rühl, E.; Flesch, R.; Tappe, W.; Novikov, D.; Kosugi, N. *J. Chem. Phys.* **2002,** 116, 3316-3322.
38. Pérez, A.; Marchán, I.; Svozil, D.; Sponer, J.; Cheatham, T. E.; Laughton, C. A.; Orozco, M. *Biophys. J.* **2007,** 92, 3817-3829.
39. Kaminski, G. A.; Friesner, R. A.; Tirado-Rives, J.; Jorgensen, W. L. *J. Phys. Chem. B* **2001,** 105, 6474-6487.
40. Wang, J.; Wolf, R. M.; Caldwell, J. W.; Kollman, P. A.; Case, D. A. *J Comput Chem* **2004,** 25, 1157-1174.
41. Mayo, S. L.; Olafson, B. D.; Goddard, W. A. *J. Phys. Chem.* **1990,** 94, 8897-8909.